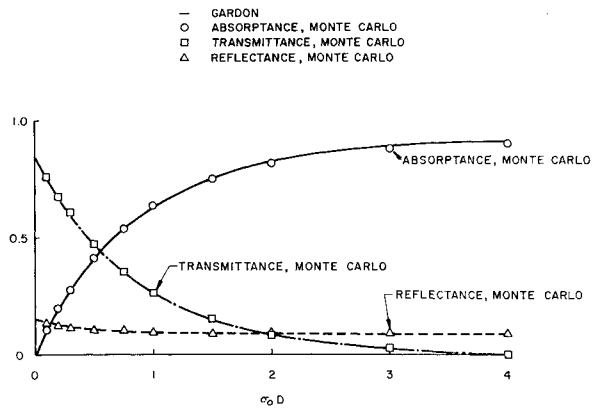

Fig. 3 Radiation properties of transparent sheet to diffuse incident radiation.

on the bottom interface as given by Eqs. (2a) and (2b), are identical to that on the upper interface since the absolute value of the sum and differences of the angles of incidence and transmission are identical for both surfaces. A third random number is picked to determine if the energy bundle is reflected from the bottom interface. If the particle is transmitted, it is counted as such. If, however, the particle is reflected, the angle of reflection will be equal to the angle of incidence β, from basic optics, and the maximum path length the particle can travel in reaching the top interface is again L. In reaching the top interface, point II, the particle will travel a total distance of $2L$. If the actual path length that the particle travels (originally greater than L) is now less than $2L$, the particle will now be absorbed. If, however, the particle reaches the top interface, it is determined whether the particle is reflected or transmitted into space. The process is repeated until the particle is either absorbed, reflected, or transmitted.

As each particle is followed, its ultimate destination is recorded. Since the final results are statistical in nature—that is, the number of particles which terminate in one position are compared to the total number of particles followed—it is necessary to determine how many histories are necessary to obtain meaningful results. Good convergence was obtained with 500 histories. However, for all the results presented in this paper, 10,000 histories per data point were used. The angular absorptance for both perpendicular and parallel polarized radiation are shown in Fig. 1. These results were compared to the analytical results for emissivity obtained by Gardon[3] for a semitransparent sheet. The angular absorptance and transmittance for diffuse radiation, which are numerically equal to one-half of the sum of their respective polarized components, are shown in Fig. 2.

To obtain the radiation characteristics of a semitransparent sheet to diffuse incident radiation, the preceding analysis has to be modified. Firstly, the angle of incidence η of the energy bundle is not a constant but must be determined by a probabilistic method. Howell shows that for diffuse emission the angle of emission is given by

$$\sin\eta = R_n^{1/2} \tag{5}$$

By direct analogy, the angle of incidence for diffuse irradiation is given by the above relationship. In addition, for each bundle of energy, the type or polarization, $\perp$ or $\|$, must be determined to calculate the interfacial reflectivities. These changes were incorporated into the previous computer program. The radiation characteristics—absorptance, transmittance, and reflectance—of a semitransparent sheet are shown in Fig. 3.

The complete radiation properties absorptance, emmitance, and transmittance of a semi-transparent sheet were determined by the Monte Carlo Technique. The absorptance values obtained by this analysis are in excellent agreement with the analytical results obtained by Gardon for emittance.

The authors have found that the adaptation of the Monte Carlo Technique as presented in this paper is one of the most powerful tools in the determination of the radiation properties of a semitransparent medium. Geometries for which an analytical solution is impossible to obtain can be analyzed by this technique.

References

[1] Howell, J. R. and Perlmutter, M., "Monte Carlo Solution of Thermal Transfer Through Radiant Media Between Grey Walls," *Transactions of the ASME, Ser. C: Journal of Heat Transfer*, Vol. 86, 1964, pp. 116–122.

[2] Howell, J. R. and Siegel, R., *Thermal Radiation Heat Transfer*, Vol. 2, SP-164, NASA, 1969.

[3] Gardon, R., "The Emissivity of Transparent Materials," *Journal of the American Ceramic Society*, Vol. 39, No. 8, 1956, pp. 278–287.

Swirling Flow through Multiple Nozzles

RICHARD H. SFORZINI*
Auburn University, Auburn, Ala.
AND
JOHN E. ESSING†
NASA Manned Spacecraft Center, Houston, Texas

Nomenclature

A, A^* = cross-sectional area and throat value
A^*_{eff} = effective throat flow area
c_f = thrust coefficient $\equiv F/P_c A^*$
c^* = characteristic exhaust velocity
D = diameter
F = thrust
J = A^*/A_p
$\dot{m}$ = mass flow rate
P = pressure
P_c = stagnation pressure at nozzle entrance
S = nozzle center displacement from chamber centerline

Subscripts

a = atmospheric condition
e,p = nozzle exit and grain port, respectively
z = condition with radial injection and maximum A_p

Introduction

FOR swirling flow in a nozzle, conservation of angular momentum requires that the swirl become more intense as the flow area decreases during passage of the particles through the convergent section of the nozzle. The intensity reaches a maximum at the throat, decreasing effective throat area, hence mass flow and thrust. Swirling discharge through a single nozzle has been treated theoretically,[1,5] and Batson and Sforzini[6] have obtained experimental confirmation of the fluid vortex structure in a choked nozzle. Lewellen et al.[4] have demonstrated that the flow upstream of the choked section is independent of downstream boundary conditions as is the case for nonswirling gas dynamics. Treatment of swirl-

Received May 18, 1970; revision received August 10, 1970. This research was performed at Auburn University in conjunction with the Master of Science in Aerospace Engineering program of John E. Essing.

* Professor of Aerospace Engineering. Associate Fellow AIAA.
† 1st Lieutenant, U. S. Air Force, Systems Engineer, LM Systems Branch, Flight Control Division.

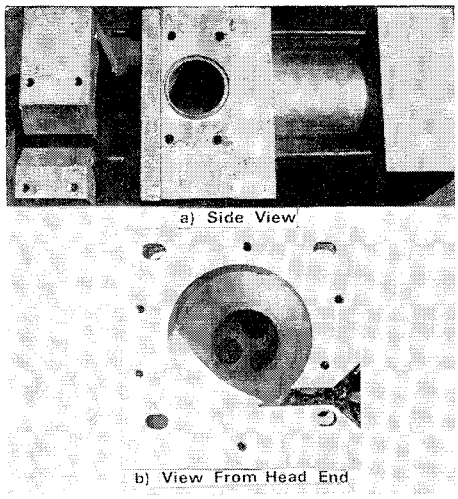

Fig. 1 Swirl chamber for nozzle flow studies.

ing flow through multiple nozzles has been scant, although Werle[7] has reported some observations regarding vortices in multiple nozzles.

The major objective of this research was to determine the effects upon thrust and mass flow of the passage of swirling flow through single and multiple nozzles of simulated solid-propellant rocket motors (SRMs). Swirling flow was induced by tangential injection of a cold gas. Although cold gas injection cannot match the characteristics of hot gases in SRMs, it is possible to establish trends with cold gas similar to those obtained with hot gases.[8] It has been demonstrated that the vortex field produced by tangential injection encompasses three distinct regions. The outer region along the tube wall is a direct result of the gas injection technique which leads to the development of a thin boundary layer along the nonrotating wall. A central or core region is formed about the motor centerline in which tangential velocity decreases with the radius until the centerline is reached. The intermediate area, which composes over 75% of the flow cross-sectional area, develops a vortex field similar to Mager's[2] free vortex model for a radially burning grain. This similarity in the intermediate area permits comparison of the stationary swirl chamber results with those of a spinning SRM with radially burning grain.[6] As a first estimate, the vortex developed by tangential injection should also approximate the nozzle flow field produced by vortex valves[4,9] or by SRMs with end-burning grains below the critical Rossby number (ratio of axial flow velocity to twice chamber wall tangential velocity).[10]

Acceleration resulting from spin also can affect the performance of SRMs by modifying the burning rate of the propellant.[11] In this Note, however, we restrict our attention to the effects of spin with respect to passage of the fluid through the nozzle.

Experimental Apparatus

The apparatus constructed to produce swirl is shown in Fig. 1. This simulated rocket motor is designed so that the internal geometry may be changed to represent SRMs with

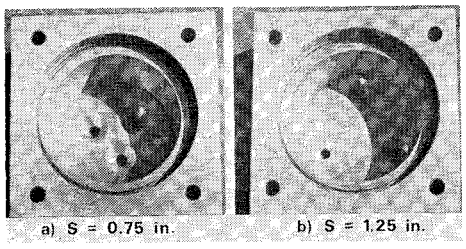

Fig. 2 Multiple nozzle test configurations.

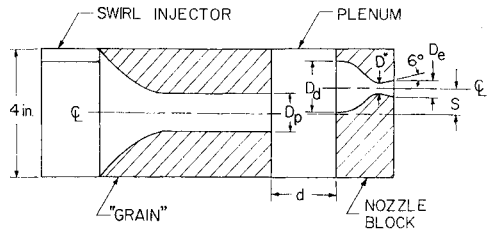

Fig. 3 Schematic of swirl apparatus with notation used in Table 1.

various ratios (J) of nozzle throat to grain port cross-sectional areas. The swirl is exhausted through sets of three nozzles displaced different distances from the model centerline in separate tests and also through a single nozzle. Three separate tangential entrance orifices made of fiberglass and resin[6] are used to produce a high, medium, and low swirl corresponding to calculated reference spin rates (based on the ratios of injection velocities to maximum chamber radius) of 138 rps, 112 rps, and 67 rps, respectively. An injection block (center of Fig. 1a) was also constructed to induce essentially axial flow into the nozzle for comparison. A chamber sleeve allows insertion of simulated combustion chambers with port diameters 4, 3, 2, 1, 0.875, and 0.750 in. The ends of the combustion chambers that fit into the chamber sleeve are machined into funnel shapes to allow for smooth flow transition to the port diameter. The two multiple nozzle configurations are shown in Fig. 2. Concurrent tests with a single nozzle at relatively large values of J not only establish reference points for comparison with the multiple nozzle but also extend some of the single nozzle results of Ref. 6 to the regime of substantial axial Mach numbers at the nozzle entrance.

Arrangement of the components is shown schematically in Fig. 3. Values of significant dimensions are given in Table 1 for the various test configurations. The swirl apparatus was attached to the settling chamber of a wind tunnel (blowdown type) air supply by a 2-in.-i.d. duct. This installation provided a supply of air at essentially ambient temperature and at a regulated pressure.

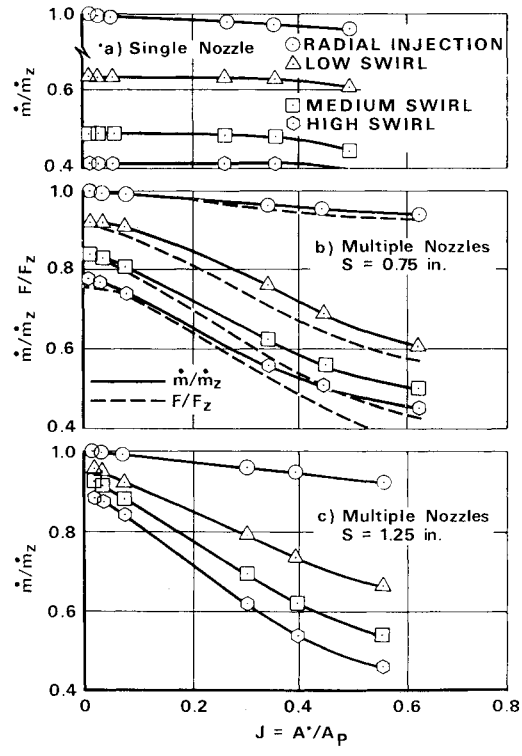

Fig. 4 Mass flow rate experimental data.

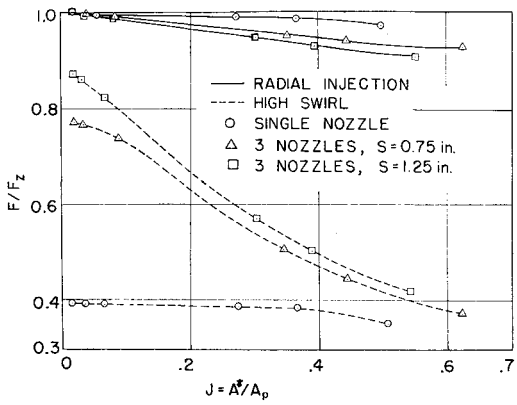

Fig. 5 Thrust results for radial and high swirl injection velocities.

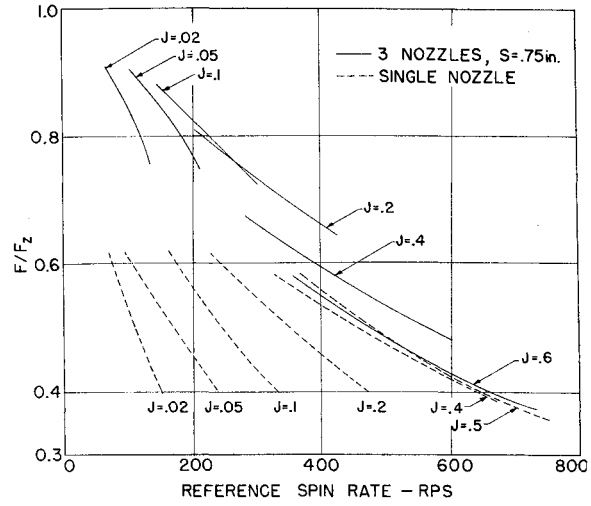

Fig. 6 Thrust vs reference spin rate.

Mass flow rates were calculated from static and total pressure and temperature measurements in the inlet duct where the flow was essentially incompressible as a result of the low velocity. A miniature probe apparatus was used for the pressure and temperature measurements.[6] Thrust measurements were obtained by the use of strain gages mounted on the inlet duct to the swirl apparatus.

Thrust and Mass Flow Results

Three tests were conducted for each of the six port areas with each of the three nozzle configurations at the three inlet swirl velocities. Average values for each test condition are reported. Measurements with radial injection were also obtained. All experiments were conducted at an inlet total pressure of 62.7 psia and a nominal total temperature of 550°R. The experimentally determined mass flow rates ($\dot{m}$'s) are given in Fig. 4. The data have been nondimensionalized by dividing by the $\dot{m}_z$ obtained for each configuration at minimum J (maximum grain port area A_p) using radial injection. Thrust curves are superimposed on Fig. 4b. These thrust curves may be considered typical in their relation to the mass flow curves although the variation between the two curves was generally somewhat less for the single nozzle and somewhat greater for the multiple nozzle with more displacement from the centerline of the swirl chamber. The thrust data presented were also nondimensionalized by dividing by the F_z corresponding to to the case of radial injection at maximum A_p for each nozzle configuration. Additional thrust data are presented in Fig. 5 for the radial injection and high swirl cases.

At maximum A_p the axial velocity in the swirl chamber is approximately 10 fps based on one-dimensional isentropic theory, and the values of F and $\dot{m}$ experimentally determined in the case of radial injection are within 4% of the values calculated by the ideal theory; i.e., the radial injection situation corresponds to predominately axial flow. Without swirl, even for the highest J's the experimentally determined F/F_z and $\dot{m}/\dot{m}_z$ correspond within 2%, which is within the probable range of experimental error for the test. When swirl is introduced, the deviation between F/F_z and $\dot{m}/\dot{m}_z$ becomes substantial as J is increased (Fig. 4b). These differences are at least qualitatively explicable in terms of reductions in A_{eff}*, as may be seen from consideration of the conventional one-dimensional isentropic relations for rocket nozzle thrust and mass flow rate[12]:

$$F = c_f P_c A^* \quad \dot{m} = P_c A^*/c^* \tag{1}$$

Swirl creates deviations from the fundamental assumptions used in obtaining Eqs. (1) because 1) exhaust gases leaving the nozzle do not have only axial velocity, and 2) gas velocity, pressure, and density are not uniform across any section normal to the flow centerline. Nevertheless, we hypothesize that the given thrust and mass flow relations remain approximately valid if suitable modifications of throat area A^*, exit area A_e, and the nozzle entrance stagnation pressure P_c are made to account for the effect of swirl. Then, application of Eqs. (1) to the present problem yields

$$(F/F_z)/(\dot{m}/\dot{m}_z) = c_f/c_{fz} \tag{2}$$

The data obtained from the experiments do not lend themselves to direct determination of effective values for A^* and A_e from which c_f may be calculated. However, comparison of the thrust and mass flow data (See Fig. 4b) shows that the ratio c_f/c_{fz} deduced by applying Eq. (2) to the test data is consistent with the reduction in c_f which would be encountered with higher effective expansion ratios as might occur at the higher swirl velocities. Higher effective expansion ratios are inferred because the percentage area reduction at the throat area plane caused by swirl will be greater than at the exit plane as indicated by the slenderness of the vortex core of low density fluid observed in Ref. 6. To check the hypothesis, values of c_f determined from Eq. (2) were used to calculate A^*_{eff}'s under the following assumptions: 1) constant effective A_e equal to the geometric A_e, and 2) P_c determined by attributing the entire difference between F and F_z in the axial flow case to losses in stagnation pressure and applying the same loss to the swirling flow data.

Kassner and Knoernschild[13] report that swirl creates up to 50% increase in friction, depending upon swirl intensity and surface roughness. Thus, the (small) P_c losses in the experimental device would be higher with the swirl. This effect, however, will tend to be offset by the smoother flow transition which accompanies the swirl between the end of the chamber port and the multiple nozzles.

Values of c_f, A_{eff}*, and P_c thus determined yield values of F as calculated from Eq. (1) which are generally 2 to 5% lower than the measured values of thrust. As an example, in the multi-nozzle with $S = 0.75$ and medium swirl, A_{eff}* ranged from 0.887 to 0.482 times the geometric A^*. In view of the

Table 1 Dimensions[a] of test configurations

Test configuration	1	2	3
Number of nozzles	1	3	3
S	0	0.75	1.25
d	0	1.75	1.75
D^*	0.520	0.330	0.312
D_e	0.580	0.369	0.349
D_d	4.00	1.00	1.00

[a] In inches; for the multiple nozzles, average values are given. See Fig. 3 for notation.

assumptions made, the experimental error, and the values of A_{eff}* calculated, the agreement between experimental and calculated thrust could hardly be fortuitous.

Direct deduction of the effect of J upon F and $\dot{m}$ in swirling flow is not possible because of the relationship between J and the swirl velocity: for one injection velocity, each value of J corresponds to a different swirl condition. To separate the effect of J, new swirl velocities were calculated for each A_p based on the assumption that potential vortex flow exists in the entrance to the simulated grain port for which

$$Vr = \text{Const} \tag{3}$$

From the swirl velocities calculated from Eq. (3) for each A_p and each injection velocity, reference spin rates were calculated. Results are given in Fig. 6, which shows that, at one spin rate, J may have a substantial effect on thrust (and $\dot{m}$). The effect is complicated: its direction and magnitude depend upon spin rate, value of J, and type of nozzle system. The reference spin rates calculated here should not be applied to systems of different scale without attention to appropriate similarity relations.

Conclusions

Tangential injection provided a method of studying swirling effects. The data obtained also allowed study of axial flow in multiple nozzles displaced various distances from the centerline. The data permit several significant conclusions: 1) As swirl intensity increases, both mass flow rate ($\dot{m}$) and thrust (F) are substantially reduced. These reductions of F and $\dot{m}$ can be explained quantitatively, using one-dimensional isentropic flow theory, as being due to an effective reduction in throat area caused by development of a low-density core. 2) For a given reference spin rate, as $J = A^*/A_p$ decreases (tangential velocity at the port radius increases), the effects depend on the type of nozzle system and the values of J and spin rate. 3) For flow in which swirl is essentially absent, thrust is slightly reduced as nozzles are displaced farther from the swirl chamber centerline for any J. The total thrust reduction is primarily a result of a total pressure drop.

The results depict the behavior of swirling and axial flow through multiple nozzles; however, methods are needed which will permit analytical determination of vortex core size and effective throat area in multiple nozzles as the analyses of Mager[2] and Norton et al.[5] have made possible for single nozzles.

References

[1] Binnie, A. M., "The Passage of a Perfect Fluid Through a Critical Cross-section or Throat," *Proceedings of the Royal Society*, Ser. A, Vol. 197, 1949, pp. 554–555.

[2] Mager, A., "Approximate Solution of Isentropic Swirling Flow Through a Nozzle," *ARS Journal*, Vol. 31, No. 8, Aug. 1961, pp. 1140–1148.

[3] Manda, L., "Spin Effects on Rocket Nozzle Performance," *Journal of Spacecraft and Rockets*, Vol. 3, No. 11, Nov. 1966, pp. 1695–1697.

[4] Lewellen, W. S., Burns, W. J., and Strickland, H. J., "Transonic Swirling Flow," *AIAA Journal*, Vol. 7, No. 7, July 1969, pp. 1290–1297.

[5] Norton, D. J., Farquhar, B. W., and Hoffman, J. D., "An Analytical and Experimental Investigation of Swirling Flow in Nozzles," *AIAA Journal*, Vol. 7, No. 10, Oct. 1969, pp. 1992–2000.

[6] Batson, J. L. and Sforzini, R. H., "Swirling Flow through a Nozzle," *Journal of Spacecraft and Rockets*, Vol. 7, No. 2, Feb. 1970, pp. 159–163.

[7] Werle, H., "Vortices in Multiple Nozzles," *La Recherche Aerospatiale*, No. 2, March 1966, pp. 31–33.

[8] Ehricke, K., "A Comparison of Propellants and Working Fluids for Rocket Propulsion," *ARS Journal*, Vol. 23, No. 5, Sept. 1953, pp. 287–300.

[9] Blatter, A. and Keranen, T. W., "A Vortex Valve for Flow Modulation of 5500°F Gas," *Journal of Spacecraft and Rockets*, Vol. 7, No. 2, Feb. 1970, pp. 169–174.

[10] Dunlap, R., "An Investigation of the Swirling Flow in a Spinning End-Burning Rocket," *AIAA Journal*, Vol. 7, No. 12, Dec. 1969, pp. 2293–2300.

[11] Anderson, J. B. and Reichenbach, R. E., "An Investigation of the Effects of Acceleration on the Burning Rate of Composite Propellants," *AIAA Journal*, Vol. 6, No. 2, Feb. 1968, pp. 271–277.

[12] Barrère, M., Jaumotte, A., Fraeijs De Veubeke, B., and Vanderkerckhove, J., *Rocket Propulsion*, Elsevier, Amsterdam, 1960, pp. 60–61, 88–89.

[13] Kassner, R. and Knoernschild, E., "Friction Laws and Energy Transfer in Circular Flow," TR F-TR-2198-ND, 1947, Wright-Patterson Air Force Base, Ohio.

Deep Space Shuttles: Chemical vs Nuclear; Direct Flight vs Near-Orbit Rendezvous

ROBERT SALKELD*

410 1/2 Landfair Avenue, Westwood Village, Los Angeles, Calif.

Nomenclature

C = standard transportation cost/lb of payload in orbit
g = acceleration of gravity
I = specific impulse
r = vehicle gross weight/burnout weight, $e^{\Delta v/gI}$
w = weight
v = ideal velocity gain
α = (cost/lb to place a stage in near orbit when it aids in its own delivery)/C_b
β = (re-entry vehicle plus payload weight)/(payload weight)
λ = stage structure factor, $w_{str}/(w_{pr} + w_{str})$
ν = (stage manufactured hardware cost/lb)/(effective boost cost/lb in orbit: C_b, αC_b, or $\alpha\beta C_b$)

Subscripts

E = expendable
R = reusable
a = ascent from near orbit to deep space orbit
b = boost to near orbit
e = direct descent to Earth
g = stage gross
n = descent to near orbit refueling
p = stage payload
pr = stage propellant
str = stage structure

Introduction

As space activities mature, and space transportation costs are reduced, it appears likely that there will be growing interest in space systems operating at ever greater distances from the Earth, in geosynchronous orbits and beyond. It is therefore appropriate to consider advanced transportation modes for delivery, return, maintenance and logistic support of deep space systems. Currently, only two alternative modes are receiving serious attention: 1) non re-enterable chemical shuttles which depart from near orbit, transfer to deep space orbit, and then return again to near orbit; and 2) solid core nuclear shuttles which operate in the same manner.

Received April 6, 1970; revision received May 22, 1970.

* Consultant. Associate Fellow AIAA.